16th World Conference on Earthquake Engineering, 16WCEE 2017
Santiago Chile, January 9th to 13th 2017
Paper N° 855
Registration Code: S- I1461314504

MODELING OF ROCKING FLEXIBLE BODIES CONSIDERING THE DEFORMABILITY OF THEIR BASE

E. Avgenakis [(1)], I.N. Psycharis [(2)]

[(1)] *PhD student, School of Civil Engineering, National Technical University of Athens, Greece, vavgen@central.ntua.gr*
[(2)] *Professor, School of Civil Engineering, National Technical University of Athens, Greece, ipsych@central.ntua.gr*

Abstract

In recent years, the need for resilient structural systems has led to a renewed interest in the use of rocking members, instead of conventional ones, for the design of earthquake resistant structures. This happens because, instead of developing damage and residual deformations, rocking members have the ability to re-center without significant damage, leading to increased structural safety and lower repair costs after the earthquake event. Furthermore, since rocking members attain their maximum strength just before the onset of rocking, they can reduce the seismic forces acting on the structure similarly to yielding members.

Although there has been extensive research on the response of unconstrained bodies allowed to rock and many analytical and experimental results and guidelines have been presented for the design of structural rocking members, it is believed that more research must be conducted on the numerical response of constrained rocking members used in structures.

Due to the constrained nature of the rocking motion of these members during an earthquake, either from additional elements such as prestressed tendons or from the surrounding frames, their response differs significantly from the response of free-standing rocking bodies. This happens because significant vertical forces may develop, which continuously alter the rocking response. One effect of these forces is that they cause deformation at the base of the body which can no longer be considered rigid and its deformability has to be taken into account for an accurate estimation of the rocking motion. Up to now, the deformability of rocking bodies was mostly considered only with what concerns their deformation along their height, while their base was considered rigid.

In this paper a new approach is proposed, which is able to take into account the deformability of the body along its height, as well as the deformation of its base during rocking. The rotations and the displacements, which originate from the rocking motion and the body's deformation, are examined for a typical problem of an elastic rocking block and formulas are presented for their calculation. The presented analysis is extended and incorporated into a macroelement, which could be used in the context of a finite element program, such as Opensees. Comparisons of the obtained results with corresponding results obtained with Abaqus show excellent agreement, while the proposed macroelement approach requires extremely low runtimes compared to conventional finite element codes.

Keywords: rocking; resilient structures; macro-element; nonlinear analysis

1. Introduction

The rocking motion of rigid bodies and structural members has recently gained an increased attention from the scientific community. Unlike members considered in classical mechanics, which can transmit tensile stresses through their base, members unrestrained or partially restrained at their base can develop only compressive stresses, while uplift occurs, altering significantly their response. When large enough horizontal forces are imposed on the member, its base partially detaches from the ground and the body rotates about one of its corners. The vertical force acts as the restoring force that tends to bring the body back to its original equilibrium position.

The inclusion of rocking members in real structures is considered a promising solution to the design of resilient structures. During a seismic event, conventional structural elements are designed to gradually yield and develop damage and residual deformations, requiring repairs afterwards. In contrast, rocking members exhibit a yield-like response, able to limit the forces transmitted to the structure during an earthquake, developing however little damage and residual deformations.

Up to date, rocking members have been applied in case of bridge piers (e.g. the Rangitikei Railway Bridge [1]), while extensive analytical and experimental work has been performed on rocking shear walls in precast structures (e.g. [2], [3], [4]). Furthermore, guidelines addressing this alternative seismic design have been published by several organizations.

Although various configurations of rocking members are examined in literature, such as the rocking motion of rigid blocks, rigid blocks on flexible foundations or rocking bodies considering the flexibility along their height (indicatively [5], [6], [7], [8], among others), few studies consider the deformability of rocking bodies along the rocking interface (e.g. [9]), although it is considered important for many practical situations.

In this paper, a new macro-element formulation is proposed, able to take into account both the deformability of the rocking member along its height and along the contact area with the base mat. The main idea behind the proposed approach is to assume a stress distribution acting on the section of the rocking interface, depending on the resultant forces on this interface, and try to predict the displacements of the rocking element due to this partial loading. To this end, the similarity between the original problem of the flexible rocking body and that of a cantilever, partially loaded on its free side with normal and shear stresses that model the ones acting on the contact region of the body while rocking (Fig. 1) is used. More information on the applied technique can be found in [10].

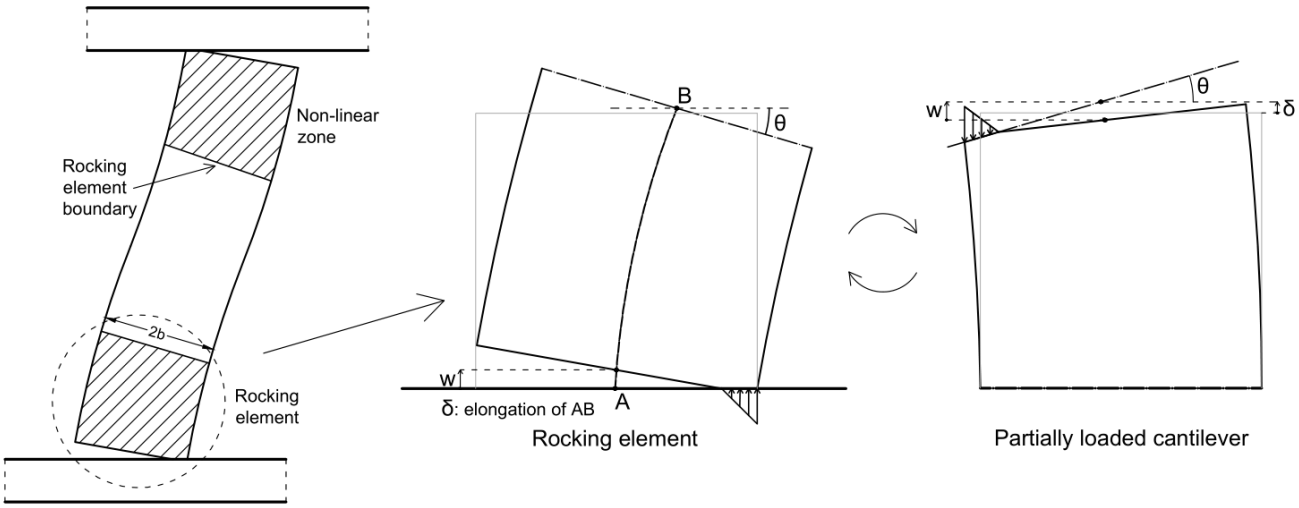

Fig. 1 – Rocking body and partially loaded cantilever analogy

2. Normalized semi-infinite strip problem

The partial loading of a cantilever on its free side produces a nonlinear stress distribution near the loaded region. After the fiber elongations due to this stress distribution are calculated, the displacements at element ends can be approximated.

In order to achieve that, the normal and shear stress distributions applied on the free side are separated into: (i) stresses produced by the resultant forces (axial force, shear force and moment); and (ii) self-equilibrating stresses. For the latter, since the effect of the self-equilibrating stresses is expected to vanish along the cantilever (rightmost diagram in Fig. 1), as the Saint-Venant assumption suggests, the easier semi-infinite strip problem is used instead. The stress distributions of the resultant forces are calculated according to the technical theory, so the use of a cantilever model is not necessary.

The general self-equilibrating stress problem for a semi-infinite strip of width $B = 2b$ is solved by first examining the normalized problem, which refers to a semi-infinite strip of $b = 1$ (Fig. 2). The self-equilibrating stress distribution problem of the normalized semi-infinite strip is calculated with the method developed in [11], using stress functions of certain form.

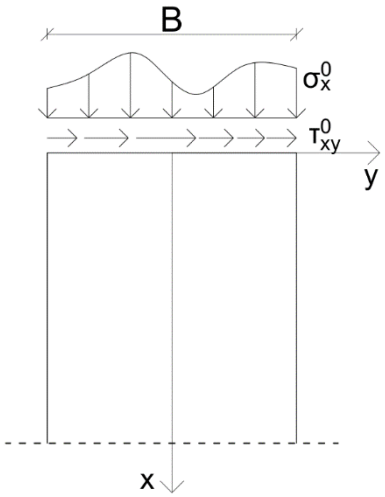

Fig. 2 – Semi-infinite strip problem

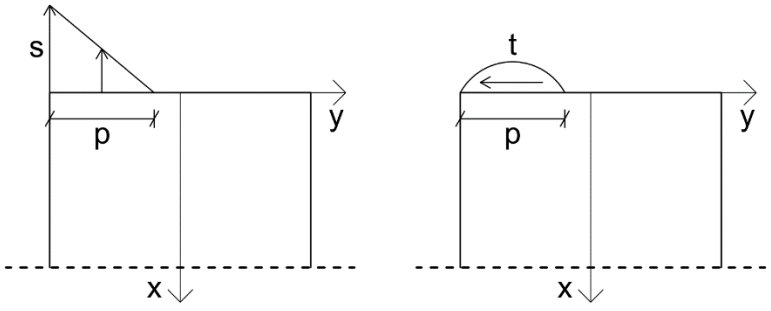

Fig. 3 – Semi-infinite strip normal (s) and shear (t) load distributions, for loaded region of length p

The free surface of the semi-infinite strip is assumed to be loaded in the interval $[-1, p-1]$, representing a contact region of length p of the corresponding rocking body (Fig. 3). This stress distribution is similar to the one of the contact stresses at the interface between the rocking body and the base and is composed of:

- *Normal stresses* which have a triangular distribution. The maximum value is s at the edge, $y = -1$, while it becomes zero after length p, that is at $y = p-1$.

- *Shear stresses* which are assumed to have a parabolic distribution. Their values are zero at $y = -1$ and $y = p-1$, while their maximum value t occurs at $y = 0.5p-1$.

The self-equilibrating stress distributions assumed for the free surface of the semi-infinite strip originate from the aforementioned ones, after the removal of the resultant forces.

After the derivation of the nonlinear stress distribution due to these loads, the elongation profile $u(y)$ of the fibers across the loaded region [-1, p-1] is interpolated by a linear function $g(y) = \delta+\theta y$ (Fig. 1), in which δ and θ are the predicted axial elongation and the top rotation of the normalized problem, respectively, taking into account the gap existing between the loaded and non-loaded surfaces (Fig. 1).

It can be proven that for the stress distributions examined, the displacement vector $\boldsymbol{U} = [\delta, \theta]^T$ can be very well approximated by the following expressions:

$$\boldsymbol{U} = \begin{Bmatrix} \frac{1}{E}\,(s\boldsymbol{V}_s^T + t\boldsymbol{V}_t^T)\,\boldsymbol{P}_6 \\ \frac{1}{E}\,(s\boldsymbol{R}_s^T + t\boldsymbol{R}_t^T)\,\boldsymbol{P}_6 \end{Bmatrix} \tag{1}$$

where

$$\boldsymbol{P}_6 = [p^6 \;\; p^5 \;\; p^4 \;\; p^3 \;\; p^2 \;\; p \;\; 1]^T \tag{2}$$

$$\boldsymbol{V}_t = \boldsymbol{V}_{t0} + \nu\boldsymbol{V}_{td} \tag{3}$$

$$\boldsymbol{R}_t = \boldsymbol{R}_{t0} + \nu\boldsymbol{R}_{td} \tag{4}$$

E and ν being the Young's modulus and the Poisson ratio, respectively, and the polynomial constant term $\boldsymbol{V}_s$, $\boldsymbol{R}_s$, for the normal stress contribution, and $\boldsymbol{V}_{t0}$, $\boldsymbol{V}_{td}$, $\boldsymbol{R}_{t0}$, $\boldsymbol{R}_{td}$, for the shear stress contribution vectors, given in Table 1.

Table 1 – Polynomial approximation constant term vectors

$\boldsymbol{V}_s$	$\boldsymbol{V}_{t0}$	$\boldsymbol{V}_{td}$	$\boldsymbol{R}_s$	$\boldsymbol{R}_{t0}$	$\boldsymbol{R}_{td}$
−0.1403784	−0.1403784	−0.1403784	−0.1403784	−0.1403784	−0.1403784
1.07433528	1.07433528	1.07433528	1.07433528	1.07433528	1.07433528
−3.2789455	−3.2789455	−3.2789455	−3.2789455	−3.2789455	−3.2789455
5.21236206	5.21236206	5.21236206	5.21236206	5.21236206	5.21236206
−5.0376812	−5.0376812	−5.0376812	−5.0376812	−5.0376812	−5.0376812
3.53446524	3.53446524	3.53446524	3.53446524	3.53446524	3.53446524
−1.5484860	−1.5484860	−1.5484860	−1.5484860	−1.5484860	−1.5484860

Also, the flexibility matrix of the normalized problem $\boldsymbol{F}_t = \partial\boldsymbol{U}/\partial\boldsymbol{R}$, with $\boldsymbol{R} = [p, s, t]^T$, is calculated by the following expression:

$$\boldsymbol{F_t} = \frac{\partial \boldsymbol{U}}{\partial \boldsymbol{R}} = \begin{bmatrix} \frac{1}{E}\,(s\boldsymbol{V}_s^T + t\boldsymbol{V}_t^T)\,\boldsymbol{dP}_6 & \frac{1}{E}\,\boldsymbol{V}_s^T\,\boldsymbol{dP}_6 & \frac{1}{E}\,\boldsymbol{V}_t^T\,\boldsymbol{dP}_6 \\ \frac{1}{E}\,(s\boldsymbol{R}_s^T + t\boldsymbol{R}_t^T)\,\boldsymbol{dP}_6 & \frac{1}{E}\,\boldsymbol{R}_s^T\,\boldsymbol{dP}_6 & \frac{1}{E}\,\boldsymbol{R}_t^T\,\boldsymbol{dP}_6 \end{bmatrix} \tag{5}$$

where

$$\boldsymbol{dP}_6 = [6p^5 \;\; 5p^4 \;\; 4p^3 \;\; 3p^2 \;\; 2p \;\; 1 \;\; 0]^T \tag{6}$$

3. Combined response

By combining the self-equilibrating stresses and the resultant force contributions, a macro-element algorithm is developed which accounts for the total response of the rocking member.

For the rocking macro-element formulation, the concept of the simply supported beam natural system is used, requiring only relative member end displacement values, which is based on the geometrically nonlinear force-based beam-column element formulation proposed by Neuenhofer and Filippou [12]. The equations for the transformation of the displacements and forces to and from the simply supported beam natural coordinate system can be found in [12].

For the normalized semi-infinite strip problem discussed in section 2, given the load parameter vector $\boldsymbol{R} = [p, s, t]^{\mathrm{T}}$, the displacements $\boldsymbol{U}$ and the flexibility matrix $\boldsymbol{F}_t$ can be evaluated, which refer to the cantilever-like reference system of the semi-infinite strip. However, in order to combine these results with the resultant-force ones, these quantities have to be converted from and to a reference system of a simply supported beam.

Additionally, the problem that was formulated in section 2 referred to a semi-infinite strip of normalized semi-width $b = 1$, thickness $W = 1$ and stress distributions defined in the range $[-1, p-1]$. So, this problem has to be generalized to cover random width B, thickness W and load direction cases.

The conversion of the simply supported beam forces, $\boldsymbol{Q'} = [Q'_1, Q'_2, Q'_3]^{\mathrm{T}}$, to the normalized problem cantilever ones, $\boldsymbol{Q'_c} = [N_c, M_c, Q_c]^{\mathrm{T}}$, to the corresponding stress load parameters, $\boldsymbol{R_c} = [c, s, t']^{\mathrm{T}}$, and finally to normalized problem stress load parameters, $\boldsymbol{R} = [p, s, t]^{\mathrm{T}}$, is described by the following equations:

$$\boldsymbol{Q'_c} = \boldsymbol{S_1}\,\boldsymbol{Q'} \tag{7}$$

$$\boldsymbol{R_c} = \left[3\left(b + \frac{|M_c|}{N_c}\right) \quad \frac{2}{3}\left(\frac{N_c}{b+\frac{|M_c|}{N_c}}\right) \quad \frac{1}{2}\left(\frac{Q_c}{b+\frac{|M_c|}{N_c}}\right)\right]^T \text{ with } N_c<0 \tag{8}$$

$$\boldsymbol{R} = \boldsymbol{S_2}\,\boldsymbol{R_c} \tag{9}$$

where

$$\boldsymbol{S_1} = \frac{1}{W}\begin{bmatrix}1 & 0 & 0\\ 0 & 1 & 0\\ 0 & -\frac{1}{L} & -\frac{1}{L}\end{bmatrix} \quad \boldsymbol{S_2} = \begin{bmatrix}\frac{1}{b} & 0 & 0\\ 0 & 1 & 0\\ 0 & 0 & \rho\end{bmatrix} \quad \text{and } \rho=\text{sign}(M_c) \tag{10}$$

Similarly, after the calculation of the displacements $\boldsymbol{U} = [\delta, \theta]^T$ of the normalized problem, the conversion to the ones of the general simply supported beam problem, $\boldsymbol{q'} = [q'_1, q'_2, q'_3]^{\mathrm{T}}$, is described by the equation:

$$\boldsymbol{q'} = \boldsymbol{S_3}\,\boldsymbol{U} \tag{11}$$

where

$$\boldsymbol{S_3} = \begin{bmatrix}b & 0\\ 0 & \rho\\ 0 & 0\end{bmatrix} \tag{12}$$

The self-equilibrating part of the rocking element is active only if a portion of the section supported on the ground is active, that is, only if

$$c < B \;\Rightarrow \left|\frac{M_c}{N_c}\right| > \frac{b}{3} \tag{13}$$

which means that the resultant normal force must be located outside the kern of the section.

Also, given the flexibility matrix of the normalized semi-infinite strip problem $\boldsymbol{F}_t = \partial\boldsymbol{U}/\partial\boldsymbol{R}$, the flexibility matrix in the simply supported beam coordinate system $\partial\boldsymbol{q'}/\partial\boldsymbol{Q'}$ is evaluated as follows:

$$\frac{\partial \boldsymbol{q'}}{\partial \boldsymbol{Q'}} = \frac{\partial \boldsymbol{q'}}{\partial \boldsymbol{U}}\frac{\partial \boldsymbol{U}}{\partial \boldsymbol{R}}\frac{\partial \boldsymbol{R}}{\partial \boldsymbol{R_c}}\frac{\partial \boldsymbol{R_c}}{\partial \boldsymbol{Q'_c}}\frac{\partial \boldsymbol{Q'_c}}{\partial \boldsymbol{Q'}} = \boldsymbol{S}_3\,\boldsymbol{F}_t\,\boldsymbol{S}_2\,\boldsymbol{S}_4\,\boldsymbol{S}_1 \tag{14}$$

with

$$\boldsymbol{S_4} = \begin{bmatrix} -3\frac{|M_c|}{N_c^2} & 3\frac{\rho}{N_c} & 0 \\ \frac{4}{c} - 6\frac{b}{c^2} & -6\frac{\rho}{c^2} & 0 \\ \frac{9}{2}\frac{|M_c|\,Q_c}{N_c^2\,c^2} & -\frac{9}{2}\frac{\rho\,Q_c}{N_c\,c^2} & \frac{3}{2c} \end{bmatrix} \tag{17}$$

The contribution of the resultant forces can be calculated as usual. The flexibility matrix of the elastic simply supported beam, taking into account shear deformation effects, is (e.g. [13]):

$$\boldsymbol{F_r} = \begin{bmatrix} \frac{L}{EA} & 0 & 0 \\ 0 & \frac{L}{3EI} + \frac{\alpha}{GAL} & -\frac{L}{6EI} + \frac{\alpha}{GAL} \\ 0 & -\frac{L}{6EI} + \frac{\alpha}{GAL} & \frac{L}{3EI} + \frac{\alpha}{GAL} \end{bmatrix} \tag{18}$$

where α is the shear shape factor with $\alpha \approx 1.2$ for rectangular cross sections (shear deformations contribution can be neglected by setting $\alpha = 0$). So, the displacements at the nodes originating from the resultant forces are given by

$$\boldsymbol{q_r'} = \boldsymbol{F_r}\,\boldsymbol{Q'} \tag{19}$$

The general algorithm for the macro-element which combines these two contributions, based on the algorithm in [12], is presented in Table 2, where index refers to the resultant force problem and refers to the self-equilibrating stress problem (extended semi-infinite strip algorithm).

In order to verify the validity of the proposed approach, the response of an elastic rocking body under a vertical and a horizontal top force (Fig. 4a) is predicted using the aforementioned algorithm and is compared against the one obtained from the corresponding Abaqus model. More specifically, apart from the pushover capacity curve (Fig. 4b), the curves presenting the vertical displacement (Fig. 4c) and the rotation (Fig. 4d) at node A are shown. It can be seen that, generally, there is very good agreement between the macroelement and the Abaqus results. The only notable difference between the two models can be seen in the vertical displacement response for large displacements. This is because the geometric nonlinearity formulation used is not exact for large displacements.

4. Example: Single-bay frame with rocking wall

In this section, the effect of the rocking of a shear wall placed at the middle of the span of a single-story, single-bay frame (Fig. 5) is examined. The wall is rocking on both the bottom and the top sides.

Results are presented for a RC frame of span length L_f = 6.0 m, with columns of cross section 0.50 m × 0.60 m and beam of cross section 0.25 m × 0.50 m, while the thickness of the rocking wall perpendicular to the frame is assumed 0.25 m. The Young's modulus of the main frame is E_f = 30 GPa, while the Young's modulus of the wall, $E_{w,}$ is considered a varying parameter. For the structural members of the frame (columns and beam), the cracked stiffness was considered, and, according to the usually made assumption (e.g. Eurocode 8 [14]) the effective stiffness was taken equal to one half of the geometric one: $EI_{eff} = 0.5 \cdot EI_g$. The vertical loads acting on the system are a distributed load q = 60 kN/m along the beam and the self-weight of the rocking wall.

In Fig. 6, the response of a frame under monotonically increasing horizontal load, P, is presented for various frame height to span length, H_f/L_f and panel width to span length, B/L_f, ratios, assuming $E_w = E_f$. Note that the case $B/L_f = 0$ corresponds to the bare frame without the wall.

Table 2 – Rocking macro-element algorithm

1. Elimination of rigid body modes	$\boldsymbol{q}_i' = \boldsymbol{T}_i\,\boldsymbol{q}_i,\ \ \Delta\boldsymbol{q}_i' = \boldsymbol{T}_i\,\Delta\boldsymbol{q}_i$
2. Nodal force increments	$\Delta\boldsymbol{Q}_i' = \boldsymbol{F}_{i-1}^{-1}\,\Delta\boldsymbol{q}_i'$
3. Nodal forces	$\boldsymbol{Q}_i' = \boldsymbol{Q}_{i-1}' + \Delta\boldsymbol{Q}_i'$
4. Flexibility matrix and Nodal displacements for the resultant force problem	$\boldsymbol{q}_r^* = \boldsymbol{F}_r\boldsymbol{Q}_i'$
5. Check whether there is rocking or not. If not, ignore steps (6)-(10) and set $\boldsymbol{q}'_s$ and $\boldsymbol{F}_s$ to the zero matrices	$\left\lvert\frac{Q_2'}{Q_1'}\right\rvert > \frac{b}{3} \rightarrow$ Rocking
6. Force parameters for the self-equilibrating stresses problem	$\boldsymbol{Q}_c' = \boldsymbol{S_1}\boldsymbol{Q}_i', \boldsymbol{R}_c = \boldsymbol{R}_c(\boldsymbol{Q}_c'), \boldsymbol{R} = \boldsymbol{S_2}\boldsymbol{R}_c$
7. Displacements of the normalized problem	$\boldsymbol{U} = \boldsymbol{U}(\boldsymbol{R})$
8. Displacements in the simply-supported beam natural system	$\boldsymbol{q}_s^* = \boldsymbol{S_3}\,\boldsymbol{U}$
9. Flexibility matrix of the normalized problem	$\boldsymbol{F_t} = \boldsymbol{F_t}(\boldsymbol{R})$
10. Flexibility matrix in the simply-supported beam natural system	$\boldsymbol{F_s} = \boldsymbol{S_3}\,\boldsymbol{F_t}\,\boldsymbol{S_2}\,\boldsymbol{S_4}\,\boldsymbol{S_1}$
11. Combined displacements	$\boldsymbol{q}_i^* = \boldsymbol{q}_r^* + \boldsymbol{q}_s^*$
12. Displacement residuals	$\boldsymbol{r}_i = \boldsymbol{q}_i' - \boldsymbol{q}_i^*$
13. Combined flexibility matrix	$\boldsymbol{F}_i = \boldsymbol{F_r} + \boldsymbol{F_s}$
14. Extra nodal forces	$\boldsymbol{Q}_i^* = \boldsymbol{F}_i^{-1}\,\boldsymbol{r}_i$
15. Updated nodal forces	$\boldsymbol{Q}_i' = \boldsymbol{Q}_i' + \boldsymbol{Q}_i^*$
16. Check convergence	$\left\lvert\frac{\boldsymbol{Q}_i^*}{\boldsymbol{Q}_i^{old}}\right\rvert >$error → return to step 4
17. Inclusion of rigid body modes	$\boldsymbol{Q}_i = \boldsymbol{T}_i^*\boldsymbol{Q}_i',\ \ \boldsymbol{K}_i = \boldsymbol{T}_{1i} + \boldsymbol{T}_i^*\boldsymbol{F}_i^{-1}\boldsymbol{T}_i^{*T}$

In Fig. 6a, the classical capacity curve is shown and it is evident that both the capacity and the stiffness increase with the ratio B/L_f, i.e. as the width B of the wall increases in comparison to the span length L_f. This behavior was expected, since rocking of the wall is more constrained by the beam for larger B's due the larger required vertical displacements of the beam, which also occur closer to its ends. Similarly, the capacity and the stiffness of the system increase as the ratio H_f/L_f decreases, i.e. as the frame becomes stiffer. Note that smaller ratios H_f/L_f also correspond to less slender walls for constant B, since the height of the wall, H, is associated with the height of the frame, H_f.

It is interesting to note that the nonlinearity of the response is mostly limited at the beginning of the response (at small drift ratios), while the post-rocking response shows a practically constant stiffness. Thus, the overall response could, in most cases, be approximated by the response of a linear system with the post rocking stiffness. This behavior is associated with the stabilization of the contact length, as shown in Fig. 6b.

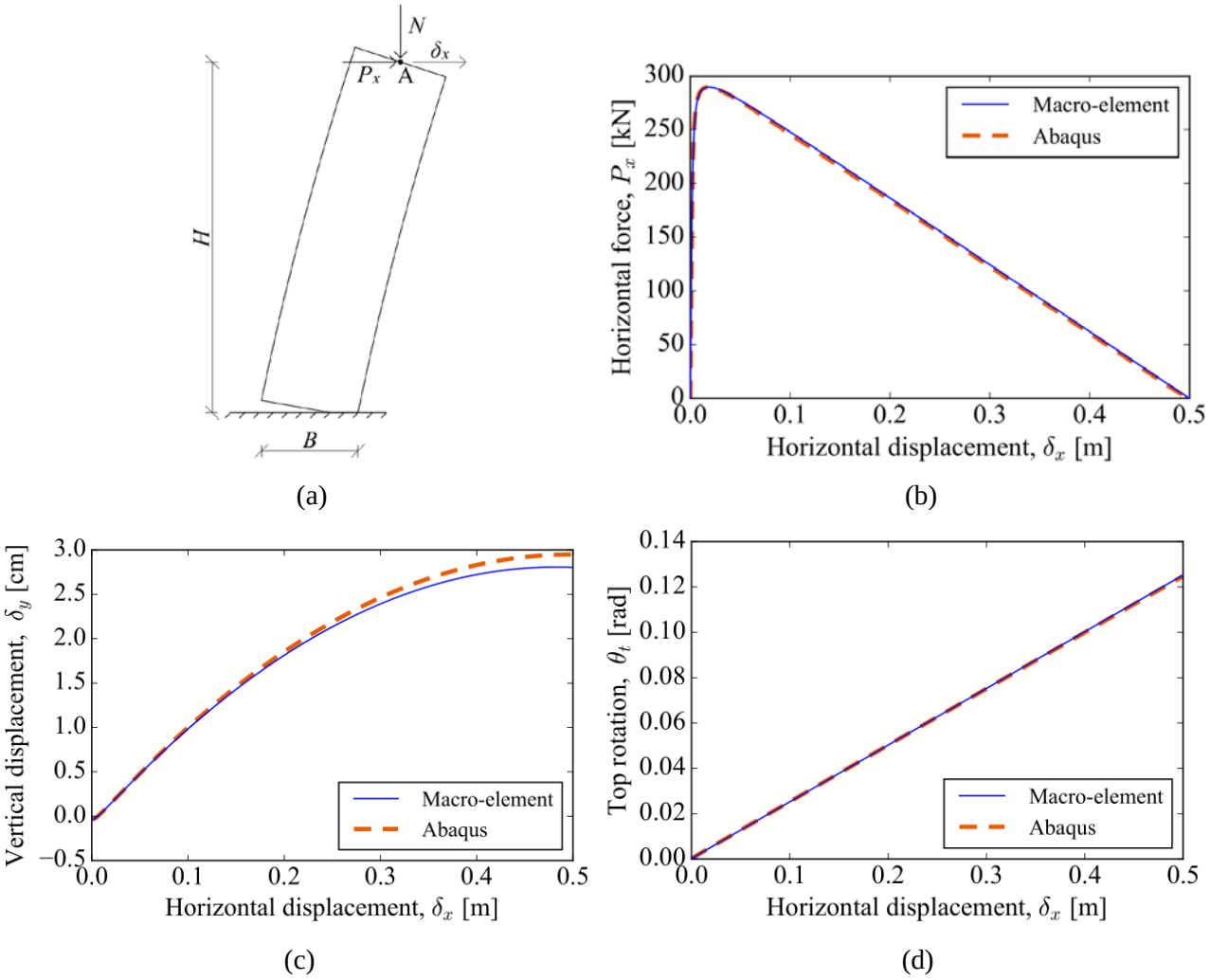

Fig. 4 – Rocking body under a vertical and a horizontal top force: (a) Model description and model deformation, (b) Horizontal force, (c) vertical displacement at point A and (d) top rotation versus horizontal displacement with the corresponding Abaqus results for E=30 GPa and ν=0.2.

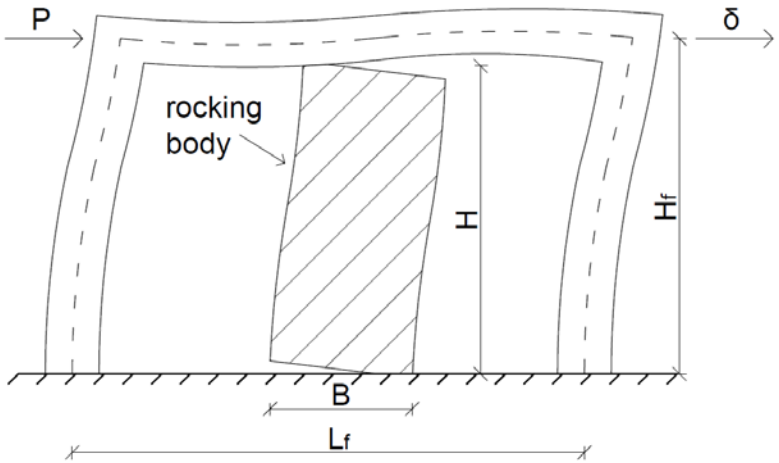

Fig. 5 – Single bay frame containing a rocking wall.

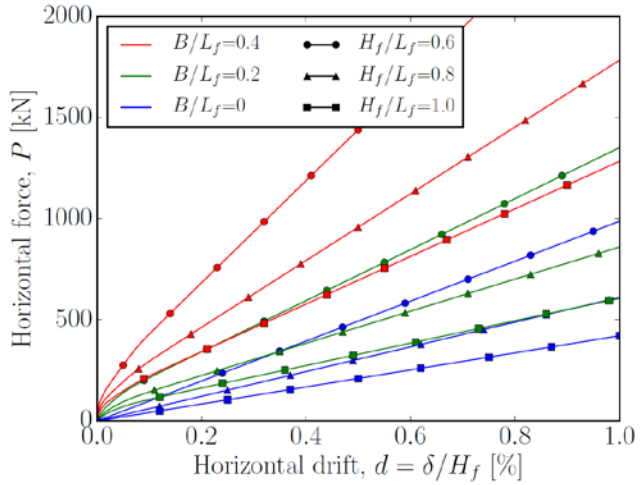

(a)

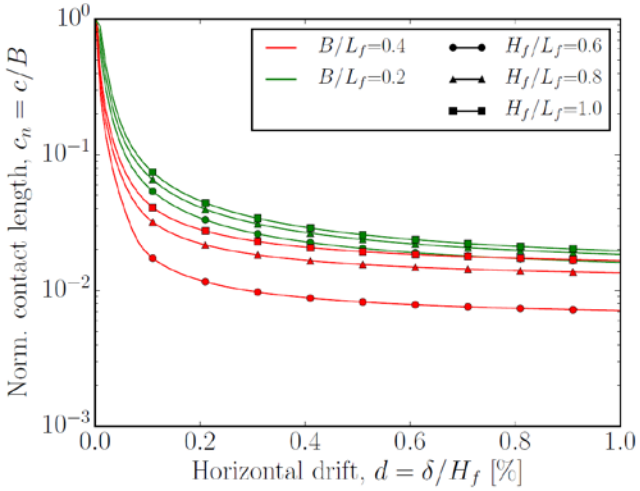

(b)

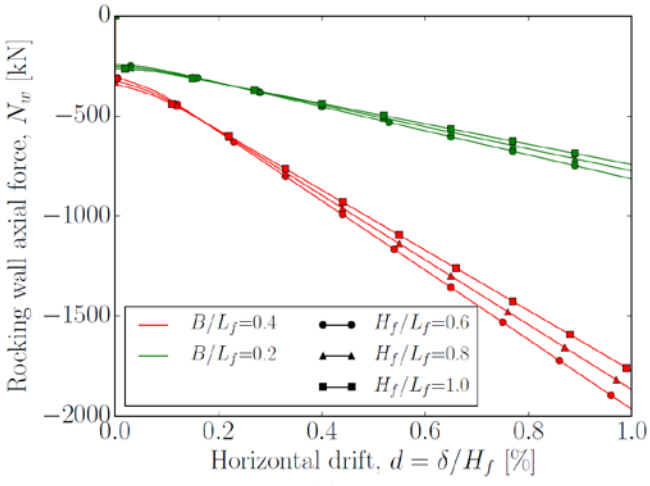

(c)

Fig. 6 – Single bay frame response curves with varying B/L_f and H_f/L_f ratios (E_w/E_f = 1): (a) Horizontal force versus drift (capacity curves); (b) Normalized contact length at the bottom side of the rocking wall versus drift for the cases examined in Fig. 6a (similar are the contact lengths at the top side; (c) Compressive axial force of the rocking wall versus drift for the cases examined in Fig. 6a.

The beneficial effect of the rocking wall to the lateral resistance of the system shown in Fig. 6a is accompanied by the disadvantageous development of tensile axial forces in the columns to balance the compressive axial force induced to the wall due to the kinematic constraints imposed by the beam. The axial force N_w that develops in the wall during rocking is shown in Fig. 6c and, as expected, it increases with B/L_f. The ratio H_f/L_f affects N_w in a much smaller degree. It is expected that, in real structures, the tensile forces induced to the columns due to the rocking wall will not increase significantly the required reinforcement, because they will be over-balanced by the gravity loads, especially at the lower stories.

In order to examine the possible benefit of the inclusion of such a rocking wall in the original frame to its seismic behavior, a response spectrum analysis is conducted, using the EC8 design spectrum for a_g = 3.6 m/s^2 and ground type B. The mass of the structure is derived taking into account the distributed load and half of the rocking member self-weight. In each case, the maximum displacement corresponding to the seismic action was calculated as the intersection of the structure capacity spectrum with the seismic acceleration – displacement response spectrum, similarly to the ATC-40 method [15], with the difference that no additional hysteretic damping was considered, since rocking does not produce such damping as the unloading path practically follows the loading one.

In Fig. 7, the maximum attainable values for various quantities for this earthquake scenario are presented with respect to the panel width to span length ratio, B/L_f. Various analyses have been performed for different frame height to span length ratios, H_f/L_f, and different panel to frame moduli of elasticity, E_w/E_f.

Concerning the base shear force (Fig.7), it is seen that the insertion of the wall does not alter it significantly. This was expected, since the total mass is about the same in all cases examined and the periods of the structure generally fall in the constant acceleration region of the design spectrum ($T_B - T_C$). Only for very stiff configurations (H_f/L_f = 0.6 and B/L_f > 0.30), for which $T_{eff} < T_B$, a reduction is observed in the base shear (Fig. 7a).

Concerning the horizontal displacements and the produced drifts, they significantly decrease as the width of the wall increases (larger B/L_f ratios) or the stiffness of the frame increases (smaller H_f/L_f ratios) (Fig. 7b). This is associated with the corresponding increase in the overall effective stiffness of the system depicted in Fig. 7c.

The axial forces induced to the wall (N_w, compressive) and the columns (N_c, tensile) are shown in Figs. 7d and 8e, respectively. Fig. 7d reveals that larger axial forces are imposed on wider rocking walls, due to the frame constraining their motion. Concerning the axial forces induced to the columns (Fig. 7e), the ones of the column which is most influenced by the rocking motion are shown. It is seen that they become tensile even for relatively narrow rocking walls and increase as the width of the wall increases. They are also larger for larger H_f/L_f ratios (less stiff frames). Such tensile forces are not expected to cause a problem in a real structure where the columns already bear significantly large compressive loads produced by the loads of the upper floors.

The main benefit of the inclusion of the rocking wall in the frame concerns the reduction in the shear forces induced to the columns, which is shown in Fig. 7f. Although for a relatively narrow wall the columns' shear force is not affected significantly or can even increase, wide walls result in a significant decrease in the shear forces of the columns, which is more pronounced as the ratio B/L_f increases.

Concerning the effect of the modulus of elasticity of the wall, the results show that, in general, differences between E_w and E_f in the order of ±25%, as the ones expected in realistic situations, do not influence the response significantly. On the contrary, H_f/L_f and especially B/L_f ratios are considered very important.

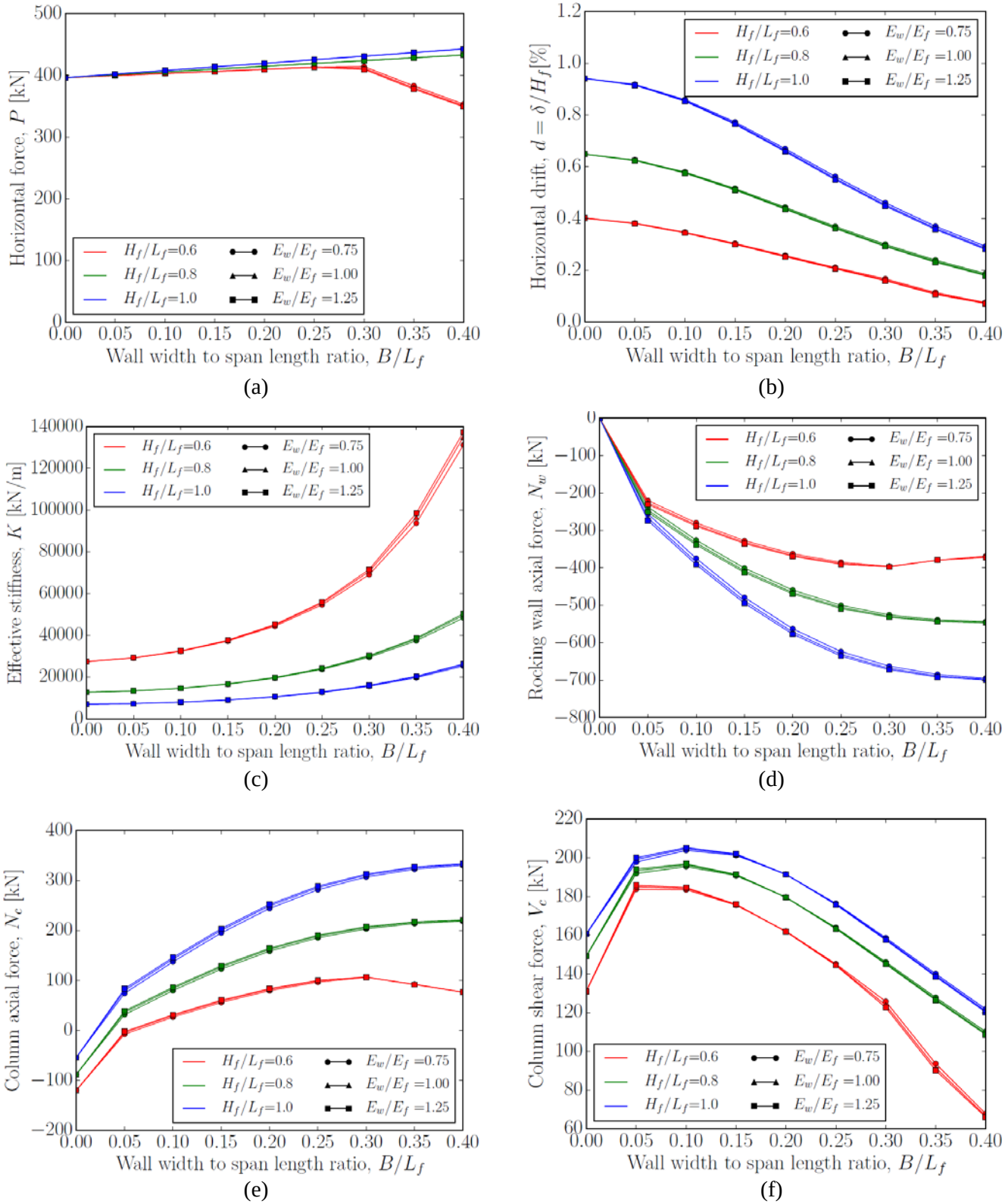

Fig. 7 – Single bay frame earthquake scenario: Maximum values with varying B/L_f ratios: (a) Horizontal force; (b) Horizontal drift; (c) Effective system stiffness; (d) Axial force induced to the wall; (e) Axial force induced to the columns; (f) Shear force induced to the columns.

5. Conclusions

In this paper, a new macro-element algorithm is presented, which can be used for the calculation of the rocking response of flexible bodies, also accounting for the deformability of their base, important in cases of restrained rocking members, when considerable axial forces develop. The main idea behind the formulation of the element is the similarity of a rocking member to that of a cantilever, partially loaded on its free side. For the latter, the semi-infinite strip problem is solved, in order to calculate the displacements of the element. Comparisons of the results produced with the macro-element for a rocking body with the ones of a corresponding Abaqus model show very good agreement.

With the help of the proposed macro-element, the nonlinear response of a single-bay frame containing a rocking wall is discussed. Such a configuration arises as a promising solution to the structural design of resilient structures, as the results present beneficial effects regarding the reduction in the drifts and in the shear forces induced to the columns. This beneficial contribution depends mainly on the ratio of the width of the wall over the frame span length, with wider rocking walls improving the seismic response significantly.

6. Acknowledgements

The first author would like to thank the Greek State Scholarships Foundation for its financial support through the "IKY Fellowships of Excellence for Postgraduate studies in Greece – Siemens program".

7. References

[1] Skinner, R., Tyler, R., Heine, A., Robinson, W. (1980): Hysteretic dampers for the protection of structures from earthquakes. *Bulletin of the New Zealand National Society for Earthquake Engineering*, **13 (**1), 22–36.

[2] Priestley, N. M. (1991): Overview of PRESSS research program. *PCI journal*, **36** (4).

[3] Sritharan, S., Aaleti, S., Thomas, D. J. (2007): Seismic analysis and design of precast concrete jointed wall systems. *ISU-ERI-Ames Report ERI-07404*, Submitted to the Precast/Prestressed Concrete Institute.

[4] Kam, W. Y., Pampanin, S., Palermo, A., Carr, A. J. (2010): Self-centering structural systems with combination of hysteretic and viscous energy dissipations. *Earthquake Engineering & Structural Dynamics*, **39** (10), 1083–1108.

[5] Housner, G. W. (1963): The behavior of inverted pendulum structures during earthquakes. *Bulletin of the seismological society of America*, **53** (2), 403–417.

[6] Yim, C.-S., Chopra, A. K., Penzien, J. (1980): Rocking response of rigid blocks to earthquakes. *Earthquake Engineering and Structural Dynamics*, **8** (6), 565–587.

[7] Psycharis, I. N. (1983): Dynamics of flexible systems with partial lift-off. *Earthquake Engineering & Structural Dynamics*, **11** (4), 501–521.

[8] Acikgoz, S. DeJong, M. J. (2012): The interaction of elasticity and rocking in flexible structures allowed to uplift. *Earthquake Engineering & Structural Dynamics*, **41** (15), 2177–2194.

[9] Roh, H. Reinhorn, A. M. (2009): Analytical modeling of rocking elements. *Engineering Structures*, **31** (5), 1179–1189.

[10] Avgenakis, E. (2015): Modeling of rocking flexible bodies considering the deformability of their base. Master's thesis, National Technical University of Athens.

[11] Gaydon, F., Shepherd, W. (1964): Generalized plane stress in a semi-infinite strip under arbitrary end-load. *Proceedings of the Royal Society of London A: Mathematical, Physical and Engineering Sciences*, **281**, 184–206.

[12] Neuenhofer, A., Filippou, F. C. (1998): Geometrically nonlinear flexibility-based frame finite element. *Journal of Structural Engineering*, **124** (6), 704–711.

[13] Przemieniecki, J. S. (1985) *Theory of matrix structural analysis*. Courier Corporation.

[14] Eurocode 8 (2004): Design of structures for earthquake resistance, Part 1: General rules, seismic actions and rules for buildings. *European Standard EN 1998-1:2004*, European Committee for Standardization.

[15] ATC-40 (1996): Seismic Evaluation and Retrofit of Concrete Buildings. Applied Technology Council (ATC).